Shape from Rotation

Richard Szeliski

Digital Equipment Corporation

Cambridge Research Lab

CRL 90/13 December 21, 1990

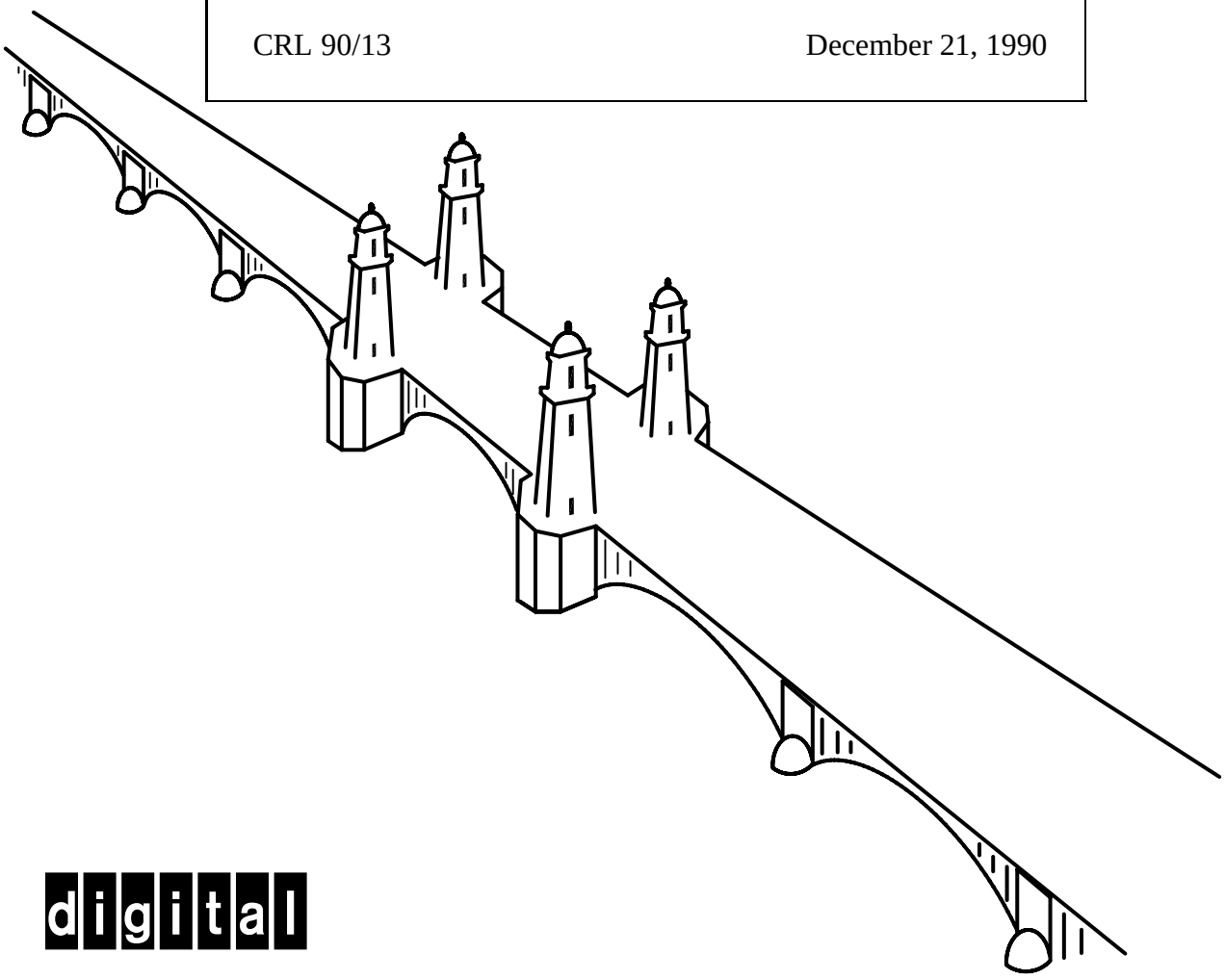

digital

CAMBRIDGE RESEARCH LABORATORY
Technical Report Series

Digital Equipment Corporation has four research facilities: the Systems Research Center and the Western Research Laboratory, both in Palo Alto, California; the Paris Research Laboratory, in Paris; and the Cambridge Research Laboratory, in Cambridge, Massachusetts.

The Cambridge laboratory became operational in 1988 and is located at One Kendall Square, near MIT. CRL engages in computing research to extend the state of the computing art in areas likely to be important to Digital and its customers in future years. CRL's main focus is applications technology; that is, the creation of knowledge and tools useful for the preparation of important classes of applications.

CRL Technical Reports can be ordered by electronic mail. To receive instructions, send a message to one of the following addresses, with the word **help** in the Subject line:

On Digital's EASYnet:	CRL::TECHREPORTS
On the Internet:	techreports@crl.dec.com

Cambridge Research Laboratory
One Kendall Square
Cambridge, Massachusetts 02139

Shape from Rotation

Richard Szeliski

Digital Equipment Corporation

Cambridge Research Lab

CRL 90/13 December 21, 1990

Abstract

This paper examines the construction of a 3-D surface model of an object rotating in front of a camera. Previous research in depth from motion has demonstrated the power of using an incremental approach to depth estimation. In this paper, we extend this approach to more general motion and use a full 3-D surface model instead of a $2\frac{1}{2}$-D sketch. The algorithm starts with a flow field computed using local correlation. It then projects individual measurements into 3-D points with associated uncertainties. Nearby points from successive frames are merged to improve the position estimates. These points are then used to construct a finite element surface model, which is itself refined over time. We demonstrate the application of our new techniques to several real image sequences.

Keywords: Computer vision, 3-D model construction, image sequence (motion) analysis, optic flow, Kalman filter, surface interpolation, computer aided design, computer graphics animation.

Contents

1 Introduction

This paper examines the construction of a 3-D surface model from image sequences of an object rotating in front of a stationary camera. Because the motion of the object between frames is known, we can use traditional depth from motion techniques to directly recover the depth of points in the image. Our approach uses a large number of images, where the motion between successive images is small. This makes it much easier to compute flow (the stereo correspondence problem is avoided), but makes individual flow measurements much less reliable. To compensate for this, we use an incremental estimation algorithm to integrate measurements from successive frames and reduce the uncertainty over time.

The incremental approach to depth estimation was previously developed by Matthies *et al.* [1989]. In this paper, we extend their work to true 3-D surface models. A simpler method for creating such models is to use the object silhouettes to "carve out" a bounding volume for the model (this method is presented in a companion report [Szeliski, 1990]). However, to obtain a more detailed description, we need to use the optic flow of the texture marks to give us a dense estimate of surface shape. Our new *shape from rotation* algorithm builds such a model, and also provides us with a framework within which we can explore a number of important issues in computer vision. These include flow estimation, uncertainty modeling, incremental estimation, 3-D surface representation and reconstruction, and massively parallel algorithms.

In addition to being an interesting research topic, the automatic acquisition of 3-D object models is important in many applications. These include robotics manipulation, where the object must first be described and/or recognized before it can be manipulated; Computer Aided Design (CAD), where automatic model building can be used as an input stage to the CAD system; and computer graphics animation or *virtual reality*, where it facilitates the task of an animator, allowing him easy access to a large catalog of real-world objects. All of these applications become much more interesting if the acquisition can be performed

quickly and without the need for special equipment or environments. Our aim is to build such a system, by using the motion of the turntable and object to provide most of the system calibration automatically. Because we also intend our system to eventually run in real-time, finding efficient parallelizable algorithms will be important.

1.1 Previous work

Some of the early work in object motion estimation [Hallam, 1983; Broida and Chellappa, 1986; Rives *et al.*, 1986; Matthies and Kanade, 1987] identified Kalman filtering as a viable framework for incremental estimation, because it incorporates representations of uncertainty and provides a mechanism for incrementally reducing uncertainty over time. Applied to depth from motion, this framework was at first restricted to estimating the positions of a sparse set of trackable features such as points or line segments [Faugeras *et al.*, 1986; Matthies and Shafer, 1987] (see also [Ullman, 1984] for an incremental approach to the related structure from motion problem). Another line of work addressed the problem of extracting denser depth or displacement estimates from image sequences (Figure 1). However, these approaches either were restricted to two frame analysis [Horn and Schunck, 1981; Anandan, 1989] or used batch processing of the image sequence, for example via line fitting [Bolles *et al.*, 1987; Baker and Bolles, 1989] or spatio-temporal filtering [Heeger, 1987]. The work of [Matthies *et al.*, 1989] overcame these limitations by combining a recursive estimation procedure with dense flow measurement. This work has recently been extended to more general motion by Heel [1990].

Because the camera motion in [Matthies *et al.*, 1989] was a pure translation perpendicular to the line of sight, the resulting image flow was always one-dimensional. Under more general camera motion, the image flow is two-dimensional and has a spatially varying uncertainty, which can be characterized using either a two-dimensional confidence measure [Anandan, 1989] or a 2×2 covariance matrix [Szeliski, 1989]. When the camera motion

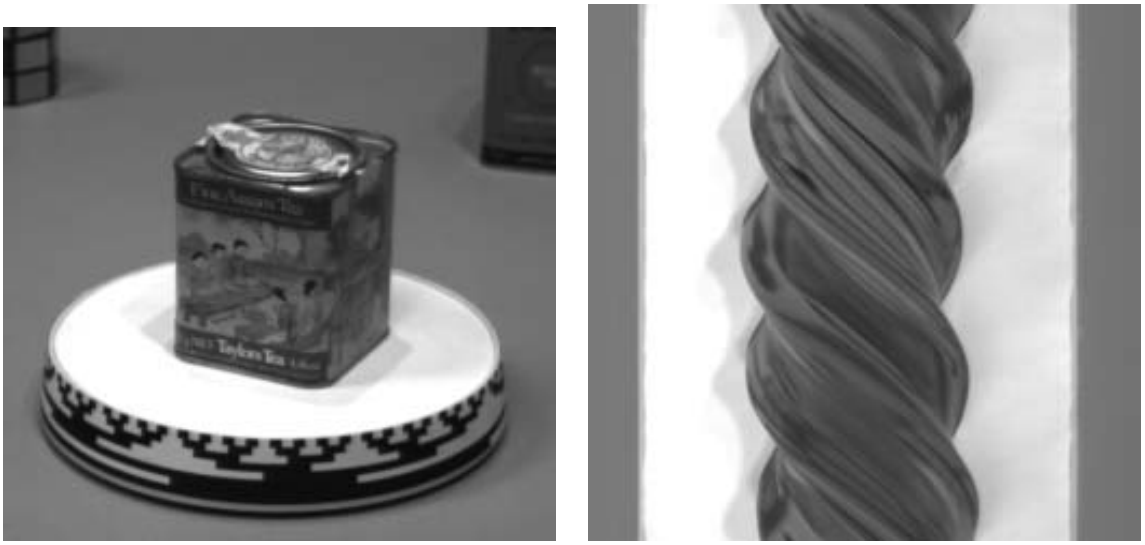

a b

Figure 1: Spatio-temporal image sequence data: (a) first image in 500 frame sequence, (b) horizontal slice through spatio-temporal cube. The average inter-frame rotation is $0.72°$.

is known, each flow measurement from the image can be converted into a 3-D position estimate in the scene, and an associated 3×3 uncertainty (covariance) matrix can be computed. As we will show in this paper, these measurements can be integrated over time (along with the intensity value associated with each points), and 3-D surfaces can be fitted to these points.

3-D shape modeling has long been one of the fundamental research areas in computer vision. The problem is to come up with representations that are sophisticated enough to model interesting objects, yet simple enough to permit recognition or construction from images or other sensor data. A variety of surface-based models have been proposed, including generalized cylinders [Brooks *et al.*, 1979], superquadrics [Pentland, 1986], and deformable finite-element models [Terzopoulos *et al.*, 1987]. Volumetric models such as octrees [Jackins and Tanimoto, 1980; Meagher, 1982] have also been used. One popular approach to constructing such volumes has been to intersect multiple silhouettes of the

object seen from different views (see [Chen and Huang, 1988; Szeliski, 1990] for a review). In this paper, we will use locally parametrized deformable surface models. Our long-term goal is to build higher-level (parts) descriptions from these surfaces.

The study of incremental shape from rotation is becoming particularly interesting because of the dramatic increase in computer processing speed, both through the availability of massively parallel architectures [Hillis, 1985], and the appearance of fast RISC microprocessors [Hennessy and Patterson, 1990]. Eventually, many of the low-level processing algorithms used in our research could be implemented using analog processing [Koch *et al.*, 1986; Hutchinson *et al.*, 1988]. One of the focuses of our research is the use of fine-grained parallel algorithms [Poggio *et al.*, 1985; Little *et al.*, 1989]. However, unlike much of the current research in low-level vision—which embeds the computation in a 2-D plane of processors—our 3-D models will require more complex representations and processor topologies.

1.2 Framework

The shape from rotation algorithm developed in this paper converts a series of images into a 3-D model of the object whose accuracy improves with time. The initial estimates of the object's shape are crude because the object motion between successive image pairs is small. Fortunately, modeling the uncertainty in these estimates allows us to refine them as more images are seen. Since we wish to build a full 3-D model, we cannot just "forget" a part of the surface when it becomes occluded. Therefore, a simple $2\frac{1}{2}$-D depth map, such as was used in [Matthies *et al.*, 1989], is not an adequate representation. On the other hand, as the object continues to rotate, we will see each view more than once, so it is not necessary to make optimal use of the information in each image.

Before we begin our 3-D surface model construction, we use a preprocessing stage to calibrate the system and to adapt to the background. The camera parameters (relative to the

turntable) are determined by imaging a known 3-D reference model such as a calibration cube (Figure 2 a). We use a binary Gray code painted on the rim of the turntable to automatically determine its rotation angle without any additional sensors (Figures 2b and 2c). These steps are described in a companion report [Szeliski, 1990], along with an algorithm for computing a bounding volume for the object from its silhouettes (Figure 2d).

The actual shape from rotation algorithm operates in the following stages. First, the 2-D optical flow between successive image pairs is extracted over the whole image (Section 2). The correlation surface corresponding to the Sum of Squared Differences (SSD) measure is used to compute both the best flow estimate at each point and its 2-D uncertainty. Next, using the known object motion, we project this flow into a 3-D position measurement with an associated 3×3 uncertainty at each point (Section 3). This "cloud" of intensity-tagged depth values is then refined by merging nearby points from successive frames whose uncertainties overlap sufficiently (Section 4). A locally parametrized surface is then fitted to this collection of points (Section 5). This stage reduces the noise in nearby measurements (using a regularization-based weak smoothness constraint [Poggio *et al.*, 1985]) and fills in the data where there is unreliable flow information (e.g., in areas of uniform intensity). The surface model, along with its associated intensities, are then refined as more images are acquired.

In Section 6 we present some experiments with real image sequences acquired in our lab. In Section 7 we compare our approach with alternative shape acquisition techniques, and we suggest a number of extensions to our work, including higher-level surface models and the merging of multiple object poses.

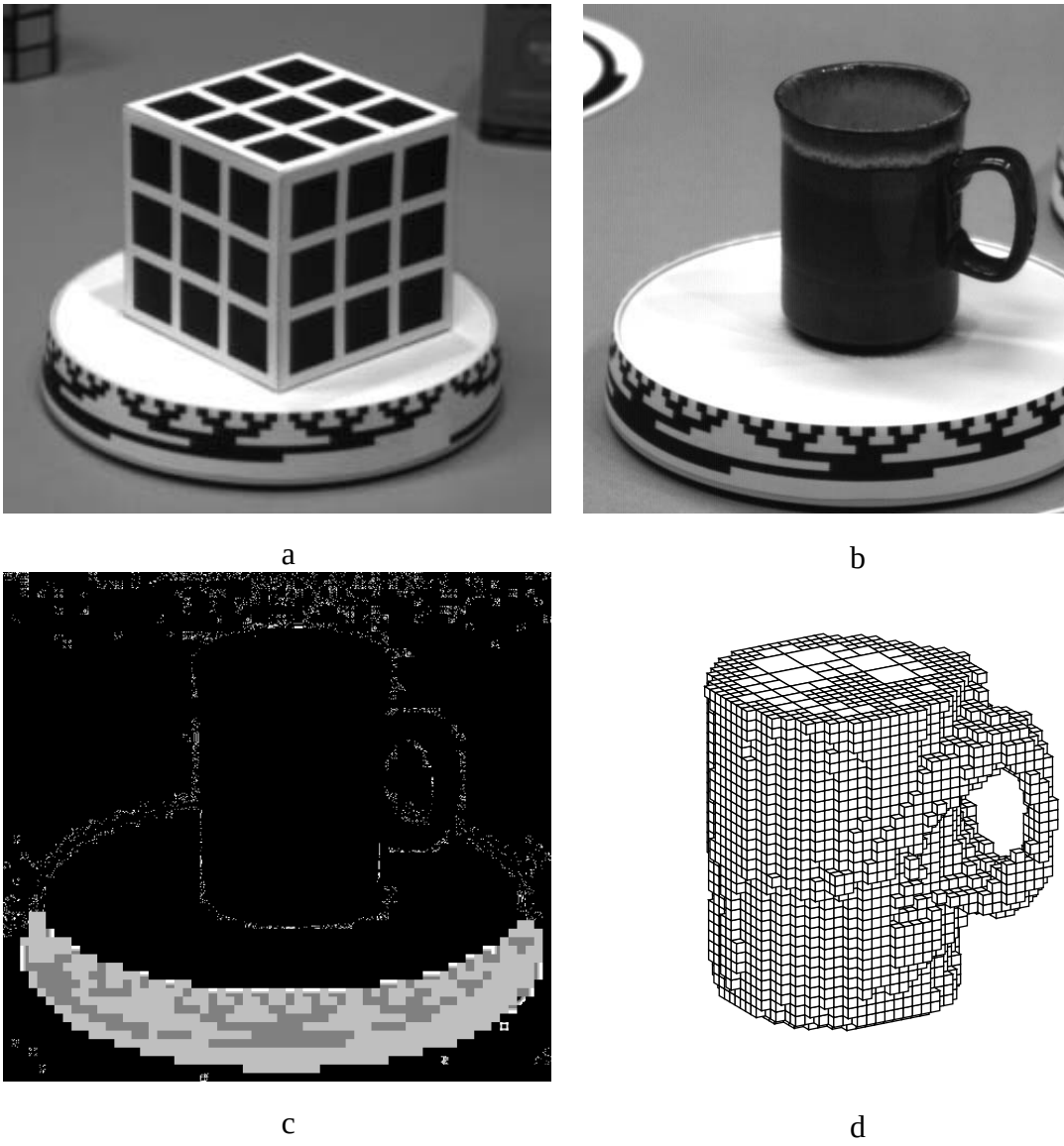

Figure 2: Image adaptation, thresholding, and bounding volume computation.
A calibration cube (a) is used to compute the camera parameters during a setup phase. Next, the system is adapted to a blank turntable to locate the Gray-code position encoding ring and to memorize the background. Each image (b) is then thresholded, yielding an object/background (black/white) segmentation (c). The Gray-code ring is used to compute the turntable angle. An incremental octree construction algorithm is used to produce the bounding volume (d). See [Szeliski, 1990] for details.

2 Optical flow

Given two or more images, we can compute a two-dimensional vector field called the *optic flow* which measures the interframe motion of each pixel in the image. A number of different algorithms have been developed previously for extracting the optic flow. In this paper, we use a variant of correlation called the *Sum of Squared Differences* (SSD) measure [Anandan, 1989], since it provides us not only with flow estimates but also with uncertainty estimates for each measurement. Alternative approaches to computing optic flow include gradient-based techniques [Horn and Schunck, 1981; Lucas, 1984; Nagel, 1987], spatio-temporal filtering [Adelson and Bergen, 1985; Heeger, 1987; Fleet and Jepson, 1989], and direct depth estimation [Heel, 1990] (see [Nagel, 1987; Anandan, 1989] for a comparison of several of these techniques).

The Sum of Squared Differences method integrates the squared intensity difference between two shifted images over a small area to obtain an error measure

$$e_t(u,v;x,y) = \int\int w(\lambda,\nu)[f_t(x+\lambda,y+\nu) - f_{t-1}(x-u+\lambda,y-v+\nu)]^2\, d\lambda\, d\nu, \quad (1)$$

where $f_{t-1}(x,y)$ and $f_t(x,y)$ are the two successive image frames, and $w(x,y)$ is a windowing function. The SSD flow estimator selects at each pixel (x,y) the flow $(\tilde{u},\tilde{v})$ which minimizes the SSD measure. In Anandan's algorithm, a coarse-to-fine technique is used to limit the range of possible flow values. In our shape from rotation work, a single-resolution algorithm is used since the range of possible motions is small.

The error surface $e_t(u,v;x,y)$ can be used not only to determine the best displacement estimate $(\tilde{u},\tilde{v})$, but also to determine the confidence in this estimate. Anandan and Weiss [1985] observed that the shape of the error surface differs depending on whether both, one, or none of the displacement components are uniquely computable (corresponding to an intensity corner, an edge, or a homogeneous area). They proposed a method for computing the confidence measures based on the principal curvatures and the directions of the principal

axes in the vicinity of the error surface minimum. Matthies *et al.* [1989] showed how for a one-dimensional displacement, the variance in the displacement estimate can be computed from the second derivative of a parabola fit to the error curve. This result was extended to two dimensions in [Szeliski, 1989], thus providing a statistical justification for the heuristics developed by Anandan and Weiss.

The derivation in [Szeliski, 1989] involves modeling the two image frames f_t and f_{t-1} as displaced versions of the same image corrupted with additive white Gaussian noise with variance σ_n^2. A quadratic of the form

$$e'_t(u,v;x,y) = \begin{bmatrix} u-\tilde{u} & v-\tilde{v} \end{bmatrix} \mathbf{A} \begin{bmatrix} u-\tilde{u} \\ v-\tilde{v} \end{bmatrix} + c \tag{2}$$

is fitted to the error surface defined by (1) by finding the values of $\mathbf{A}$, $\tilde{u}$, $\tilde{v}$, and c which minimize the weighted least squared error from the measured $e(u,v;x,y)$ values. We then set the disparity estimate at (x,y) to $(\tilde{u},\tilde{v})$, and set the variance of this measurement to $2\sigma_n^2\mathbf{A}^{-1}$. This simple model does not account for occlusions, disparity gradients or other optical effects. It is thus only valid over small windows, and breaks down in certain areas such as at occlusion boundaries. In the context of shape from rotation, we expect the flow estimates to be most reliable when a surface point is locally translating in front of the camera, and less reliable as it recedes and disappears (because of excessive warping and occlusion effects)[1]. The analysis presented in [Szeliski, 1989] can also be used to derive the correlation between adjacent flow estimates and between flow estimates obtained from successive frames.

To help differentiate between pixels which are part of the object and those in the background, it may be useful to distinguish valid flow measurements on the object's surface from all other measurements. A very simple approach to this problem is to use the

[1] Under rotation, almost every image patch is warping (undergoing a non-translation affine transformation) at every instant. However, the amount of this warping is usually very small if the images are tightly spaced in time.

background values before the object was placed on the turntable to threshold the image into foreground and background regions [Szeliski, 1990]. This approach will often fail, however, due to effects such as shadows, specularities, and nearby object/background gray levels. Another approach is to detect areas with zero optical flow by computing the SSD measure for $(u, v) = (0, 0)$ and classifying the pixel as background if this is smaller than any other SSD value. This test may fail to find some background pixels (because of imaging noise), and may erroneously classify some object pixels as background pixels, either in homogeneous areas, or at points where the motion is purely vertical (points lying on a plane parallel to the image plane passing through the rotation axis). The latter kind of error is fairly harmless, since we do not require or even expect a truly dense estimate of flow over the whole objects (e.g., areas of constant intensity will always yield little or no information).

Two additional indicators for suspect flow values suggested by Anandan [1989] are a high value for the minimum of $e_t(u, v; x, y)$, and a difference in shape between $e_t(u, v; x, y)$ and the image autocorrelation at (x, y). In practice, we have found it unnecessary to explicitly compute regions of zero or bad flow, since we can use the temporal integration phase (Section 4) to discard erroneous measurements.

3 Constrained flow and depth recovery

The general 2-D flow estimator described in the previous section is a useful first step in determining shape from motion when the object motion (*egomotion*) is unknown. In shape from rotation, however, we know the angular position of the turntable in each frame, and therefore the relative 3-D motion of the object (or equivalently, of the camera). This makes the problem of depth recovery easier, and obviates the need for additional assumptions such incremental rigidity [Ullman, 1984]. Using the known motion, we can compute for each pixel a constraint line for the flow at that point, with the actual (ideal) flow observed

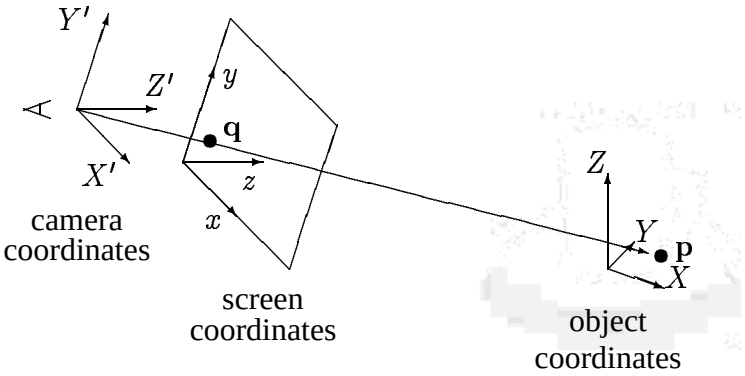

Figure 3: Object, camera, and screen coordinates

depending only on the depth of the surface at that pixel. Furthermore, we can compute a bounded segment for each flow constraint line from the minimum and maximum expected depth values (e.g., from a bounding volume or cylinder).

The simplest way to compute these constraint lines is to use homogeneous coordinates [Newman and Sproull, 1979]. Given a point in object-space $\mathbf{p} = (X, Y, Z, 1)$, we can convert it to screen coordinates $\mathbf{q} = (x, y, z, 1)$ using a linear matrix transform $\mathbf{M}$ followed by a projection operation $\mathcal{P}$ (Figure 3). First, we multiply $\mathbf{p}$ by $\mathbf{M}$ to obtain the camera-based coordinates $\mathbf{p}'$,

$$\mathbf{M}\mathbf{p} = \begin{bmatrix} X' \\ Y' \\ Z' \\ W' \end{bmatrix} = \mathbf{p}'. \tag{3}$$

The transformation matrix $\mathbf{M}$ encodes all of the information about the perspective and screen transformations such as the focal length and the aspect ratio. Next, we use the parameter-free projection operator $\mathcal{P}$ to compute $\mathbf{q}$,

$$\mathcal{P}(\mathbf{p}') \equiv \frac{1}{W'}\mathbf{p}' = \begin{bmatrix} X'/W' \\ Y'/W' \\ Z'/W' \\ 1 \end{bmatrix} = \mathbf{q}. \tag{4}$$

The above equations describe the *forward projection* from 3-D object space to screen (image) space. If we know the *depth buffer* value z for a given pixel (x, y), we can recover its 3-D location using *backprojection* (Appendix A),

$$\mathbf{p} = \mathcal{P}\left(\mathbf{M}^{-1}\mathbf{q}\right). \tag{5}$$

Computing the flow constraint line for each pixel is therefore straightforward. From our knowledge of the camera calibration and turntable rotation, we can precompute the projection matrices $\mathbf{M}_{t-1}$ and $\mathbf{M}_t$ for the previous and current frames. A pixel in the current frame $\mathbf{q}_t$ should appear at

$$\mathbf{q}_{t-1} = \mathcal{P}\left(\mathbf{M}_{t-1}\mathcal{P}\left(\mathbf{M}_t^{-1}\mathbf{q}_t\right)\right) = \mathcal{P}\left(\mathbf{M}_{t-1}\mathbf{M}_t^{-1}\mathbf{q}_t\right) \tag{6}$$

in the previous frame (Appendix A). Of course, for each pixel, we do not know the correct value of z_t, but we can project the minimum and maximum expected depth values z_t^- and z_t^+ (e.g., from the depths at the front and back of the turntable). We therefore obtain two endpoints $(x_{t-1}^-, y_{t-1}^-, z_{t-1}^-)$ and $(x_{t-1}^+, y_{t-1}^+, z_{t-1}^+)$ for the segment describing the expected previous point position. This constrains the possible flow values to lie on a line between $(u^-, v^-) = (x_t - x_{t-1}^-, y_t - y_{t-1}^-)$ and $(u^+, v^+) = (x_t - x_{t-1}^+, y_t - y_{t-1}^+)$.

Figure 4 shows a set of flow constraint segments computed for the standard imaging setup shown in Figure 1 and a 2° rotation of the turntable. Notice how the flow is generally upward at the right edge of the image and downward at the left edge. This is as expected for a scene spinning counterclockwise in front of the camera. Notice also how the flow constraint lines in a given row line up almost perfectly. This effect is even more pronounced for the smaller rotations (0.5° to 1.5°) which we use in practice.

In the case of general motion, the flow constraint line at each pixel defines the (u, v) values along which $e(u, v; x, y)$ should be searched for a minimum. For our particular imaging setup—with the vertical axes of the camera and turntable aligned, and small inter-frame displacements—we can use a near-epipolar line constraint to further reduce the

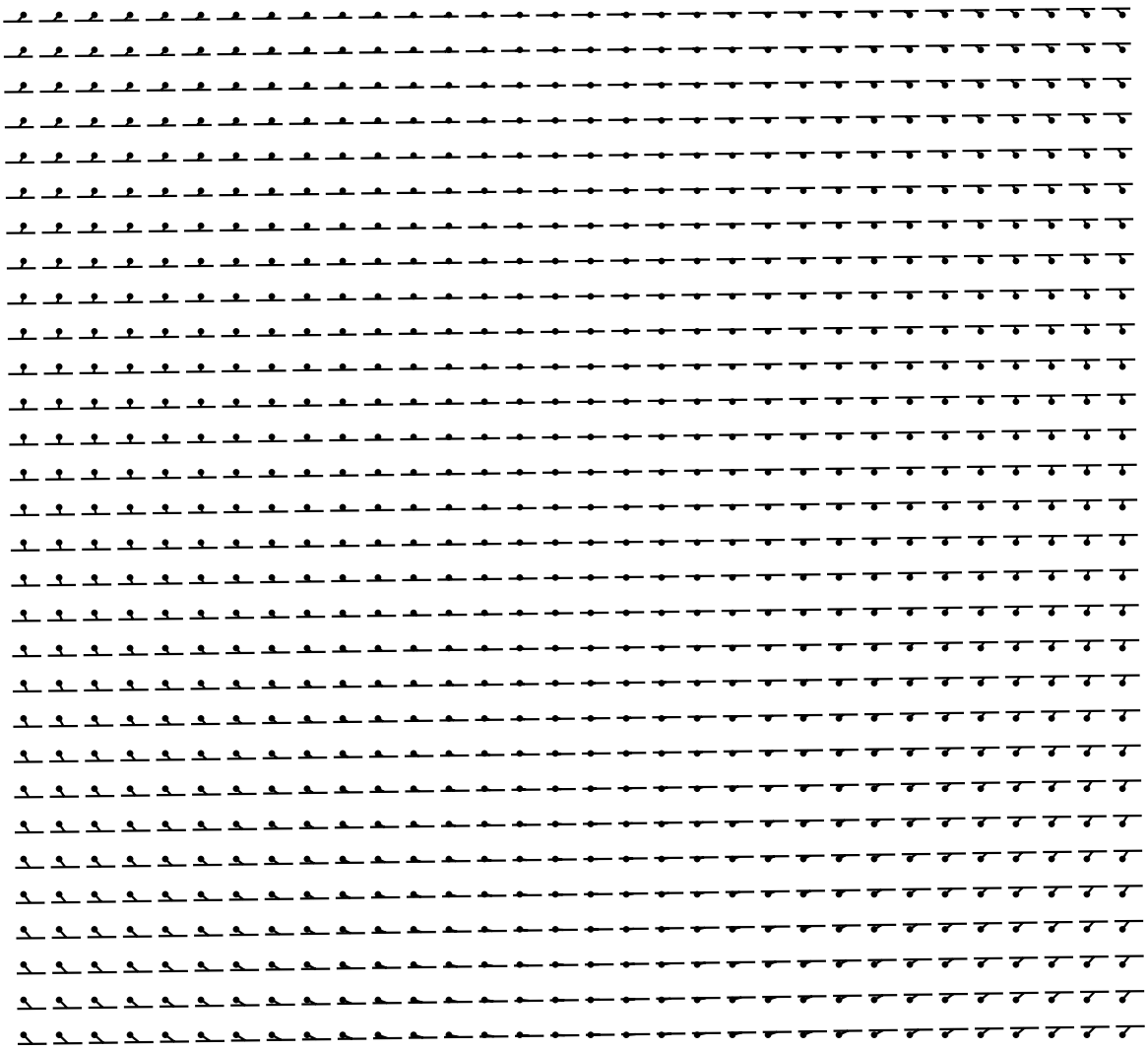

Figure 4: Flow constraint segments for 2° rotation. The dot indicates the pixel center (subsampled every 16th pixel), and the two ends of the tee indicate the minimum and maximum expected flow values.

computational complexity of our algorithm and to make it more regular. For each pixel in a given row of the current image, the pixel corresponding to a zero horizontal displacement $(0, v)$ is extracted from the previous image, thus forming the approximate epipolar line[2]. The two rows are then passed to a 1-D flow extraction algorithm similar to that used in [Matthies *et al.*, 1989], which we describe below.

The flow extraction algorithm we use is designed to compute the flow estimate $\tilde{u}$ to sub-pixel (floating-point) precision, and a confidence (variance) estimate for this measurement. Each row is first interpolated by a factor of $r = 4$ using a Hermite cubic interpolator [Szeliski and Ito, 1986] resulting in a smoother error surface at each point. For each horizontal displacement in the range $[u^-, u^+]$ (in $1/r$ steps), the discrete squared difference measure is computed

$$e(u; x) = \sum_{k=\lfloor -r/2 \rfloor}^{\lfloor (r-1)/2 \rfloor} [g_t(rx + k) - g_{t-1}(r(x - u) + k)]^2,$$

where $g_t(x)$ and $g_{t-1}(x)$ are the interpolated rows. The weighted summation over a square patch is implemented using iterated two-dimensional box filtering [Burt, 1981]

$$e^{(i)}(u; x, y) = \frac{1}{9} \sum_{k=-1}^{1} \sum_{l=-1}^{1} e^{(i-1)}(u; x + k, y + l).$$

This gives us a discrete approximation to the SSD measure at each pixel.

To extract the horizontal component of the flow at each pixel, we find the discrete value u_{min} which minimizes $e(u; x, y)$. A parabola fit to the three points $e(u_{min} - 1; x, y)$, $e(u_{min}; x, y)$, and $e(u_{min} + 1; x, y)$,

$$e(u; x, y) = a(u - u_{min})^2 + b(u - u_{min}) + c, \tag{7}$$

(Figure 5) is used to compute the sub-pixel flow estimate

$$\tilde{u} = u_{min} - b/2a \tag{8}$$

[2]Since we know the motion between the two frames, i.e., we know the *relative orientation* [Horn, 1990] of the two cameras, we could instead use the standard epipolar geometry to find the set of corresponding epipolar lines in the two images [Bolles *et al.*, 1987].

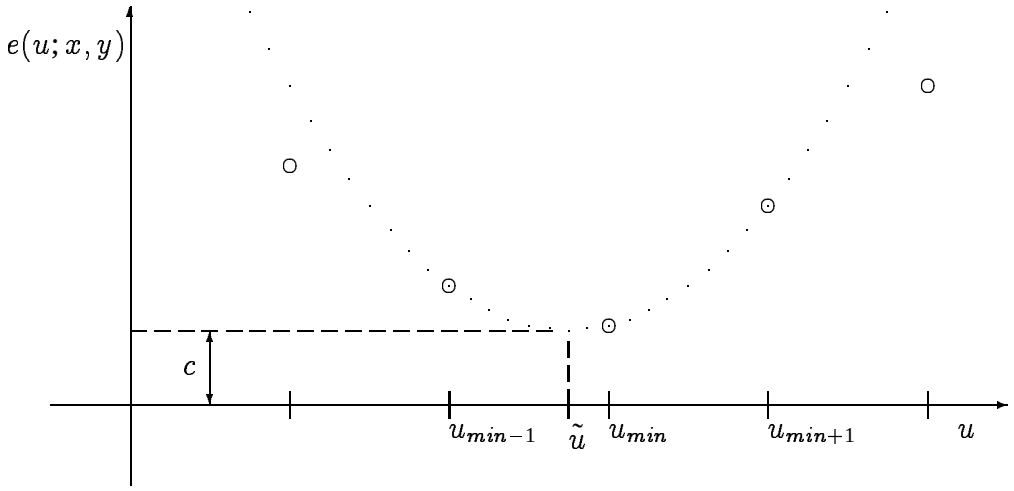

Figure 5: Parabolic fit to SSD error surface. The large circles indicate discrete values of $e(u;x,y)$; the dotted line is the parabola fit to the three lowest values.

and its variance

$$\sigma_u^2 = 2\sigma_n^2/a, \tag{9}$$

where σ_n^2 is the variance of the image noise [Matthies *et al.*, 1989]. The image noise can be estimated locally using $\sigma_n^2 = c/2$, which has the advantage of increasing the flow variance estimate in regions with a large minimum SSD value.

Once the flow estimate has been determined from the image pair, we can compute the current screen depth z_t by linear interpolation

$$z_t = z_t^- + \frac{z_t^+ - z_t^-}{u^+ - u^-}(u - u^-) \tag{10}$$

and the variance in this estimate from

$$\sigma_{z_t}^2 = \left(\frac{z_t^+ - z_t^-}{u^+ - u^-}\right)^2 \sigma_u^2. \tag{11}$$

This gives us a dense estimate of depth and uncertainty at each pixel in the image. At this point, we could throw away the measurements corresponding to background points,

occlusion boundaries, and homogeneous areas by thresholding on the variance. We could also try to reduce the noise in the depth measurements by using regularization-based smoothing, as was done in [Matthies *et al.*, 1989]. In our current experiments, we are able to obtain good results without the use of either background point removal or image-based smoothing. It remains to be seen if these additional steps would improve the quality of our estimates.

To convert these screen-based measurements $\mathbf{q}_t = (x_t, y_t, z_t, 1)$ into 3-D object space locations $\mathbf{p}_t = (X_t, Y_t, Z_t, 1)$, we use backprojection

$$\mathbf{p}_t = \mathcal{P}\left(\mathbf{M}_t^{-1}\mathbf{q}_t\right).$$

This gives us a collection of points in 3-space consistent with the flow measurements we computed.

For each 3-D point, we also need to compute a 3×3 covariance matrix

$$\mathbf{C}_{\mathbf{p}_t} = \left\langle (\mathbf{p}_t - \overline{\mathbf{p}_t})(\mathbf{p}_t - \overline{\mathbf{p}_t})^T \right\rangle,$$

which characterizes the shape and magnitude of the point's positional uncertainty. Computing this covariance matrix is tricky, since the projection operator is non-linear. If the covariance in the original measurement $\mathbf{C}_{\mathbf{q}_t}$ is sufficiently small, we can use the approximation

$$\mathbf{C}_{\mathbf{p}_t} \simeq \left(\frac{\partial \mathbf{b}}{\partial \mathbf{q}_t}\right) \mathbf{C}_{\mathbf{q}_t} \left(\frac{\partial \mathbf{b}}{\partial \mathbf{q}_t}\right)^T, \tag{12}$$

where

$$\mathbf{b}(\mathbf{q}) = \mathcal{P}\left(\mathbf{M}_t^{-1}\mathbf{q}\right)$$

is the backprojection operator (the Jacobian $\partial \mathbf{b}/\partial \mathbf{q}_t$ can be decomposed into a gradient of the projection operator times the inverse transform matrix $\mathbf{M}_t^{-1}$). In the above formula, we set the positional uncertainty in x and y to some small value (for example, $\sigma_x^2 = \sigma_y^2 = (\frac{1}{2}\text{ pixel})^2$).

A simpler approach, which we used in our experiments, is to backproject the original point plus one standard deviation $\mathbf{q}_t^* = (x_t, y_t, z_t + \sigma_{z_t}, 1)$ to get the vector

$$\mathbf{r}_t = \mathbf{p}_t^* - \mathbf{p}_t = \mathcal{P}\left(\mathbf{M}_t^{-1}\mathbf{q}_t^*\right) - \mathcal{P}\left(\mathbf{M}_t^{-1}\mathbf{q}_t\right). \tag{13}$$

This vector is the major axis of the covariance ellipsoid. The other two axes of the ellipsoid $\mathbf{s}_t$ and $\mathbf{t}_t$ can be chosen arbitrarily and their length (standard deviation) set to a suitably chosen constant value σ_0 (say, corresponding to the size of a $1/2$ pixel projected into the middle of the object). We can then form the covariance matrix using

$$\mathbf{C}_{\mathbf{p}_t} = \mathbf{R}_t\mathbf{R}_t^T \quad \text{with} \quad \mathbf{R}_t = \left[\begin{array}{c|c|c} \mathbf{r}_t & \mathbf{s}_t & \mathbf{t}_t \end{array}\right]. \tag{14}$$

Note that since $\mathbf{C}_{\mathbf{p}_t}$ can be derived from $\mathbf{r}_t$ and σ_0, it is sufficient to keep a list of $\{(\mathbf{p}_t, \mathbf{r}_t)\}$ vector pairs to fully describe the locations and uncertainties of the points computed from the current optic flow field.

4 Incremental estimation (points)

The result of our two-frame optic flow analysis and backprojection into object space gives us a "cloud" of uncertainty-tagged points lying on the surface of the object (each point also carries along with it the intensity of the associated pixel[3]). As the object continues to rotate and more points are acquired, point collections from successive frames must be merged in order to reduce the noise in point location estimates. Our collection of 3-D surface points is a less restrictive representation than the previously used depth map representation [Matthies *et al.*, 1989; Heel, 1990], which would not allow us to build a full 3-D model since it is univalued at each image pixel.

To represent the 3-D position of the points, we use an *object-centered* coordinate reference frame rather than a camera-centered frame. The origin of this frame is fixed to the

[3] In theory, we could estimate the covariance between the intensity and the point location (x, y) from the local gradient.

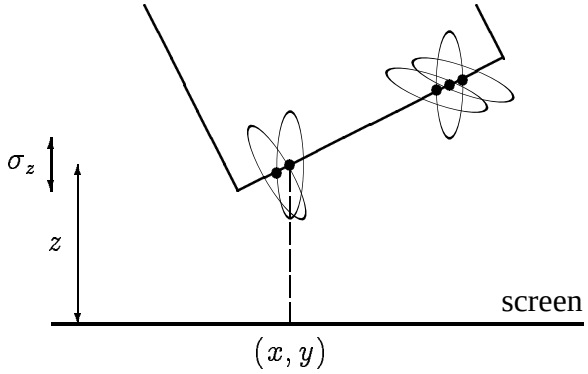

Figure 6: Merging uncertainty ellipses.

top of the turntable and rotates with it (Figure 3). This makes the estimates of 3-D position much more reliable, especially when information is being integrated over multiple frames [Tomasi and Kanade, 1990].

The question of how and when to merge neighboring 3-D points from different frames is in general quite difficult. We start by using an uncertainty-weighted distance measure

$$d_{ij} = (\mathbf{p}_i - \mathbf{p}_j)^T (\mathbf{C}_i^{-1} + \mathbf{C}_j^{-1})(\mathbf{p}_i - \mathbf{p}_j). \tag{15}$$

If this distance is sufficiently small, we can merge the two points and replace them with a single measurement

$$\mathbf{p}_k = \mathbf{C}_k(\mathbf{C}_i^{-1}\mathbf{p}_i + \mathbf{C}_j^{-1}\mathbf{p}_j) \tag{16}$$

with a reduced uncertainty

$$\mathbf{C}_k = (\mathbf{C}_i^{-1} + \mathbf{C}_j^{-1})^{-1}. \tag{17}$$

The problem with this approach is that there may be many candidate matches for a given point, especially if one elongated uncertainty ellipsoid overlaps several other points (whose own ellipsoids are distinct). Consider for example the points in the upper right of Figure 6. The points with the nearly horizontal uncertainty ellipses were measured much earlier, and the rotation of the turntable has rotated their ellipses. It is unclear with which point(s) the new measurement (with the vertical uncertainty ellipse) should be merged. It is better to inhibit merging in this case, since we cannot determine which match is correct.

A simpler and more conservative combination rule is to limit merges to points whose uncertainty ellipsoid major axes are nearly parallel and which also meet the previous distance criteria (middle of Figure 6). In this case, it is much easier to determine which of the nearby points is the best candidate for a merge. In practice, we make the merging step even simpler by re-projecting the 3-D locations and their uncertainties into the camera image plane ((x, y, z) and σ_z in Figure 6). Two points are merged if their image plane centers lie within a small distance of each other (say, $1/2$ pixel) and their depths overlap sufficiently (using a 1-D version of the uncertainty-weighted distance). The thresholds for merging points are set high enough so that neighboring measurements from the same frame are not merged (we want our final model to be at least as accurate as the input image) but low enough so that oversampling (the density of 3-D points per image pixel) is not too great.

This simplified framework has two additional advantages. First, the image plane can be used as a natural binning structure to group nearby points together for merging. Second, we can continue to use the $\{(\mathbf{p}_t, \mathbf{r}_t)\}$ (location + 1-D uncertainty) representation for all of the 3-D points. What we give up in this case is the ability to increase the resolution in the point locations orthogonal to $\mathbf{r}_t$ over time (e.g., if the points in the upper right of Figure 6 had been merged, the uncertainty would be small in all directions). This is not a problem, however, because our surface interpolation stage will smooth the surface and further reduce the positional uncertainty.

5 Local surface fitting

Once the 3-D point estimates acquired from multiple frames have been integrated sufficiently to make them reliable, we can start building a 3-D surface model. This model serves both to reduce the noise in the position estimates (through smoothing) and to fill-in areas on the object surface where no reliable flow information is available. The 3-D surface model

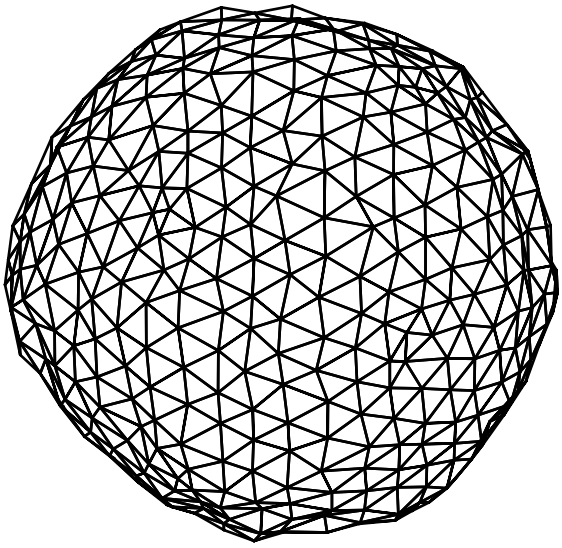

Figure 7: A 3D surface model. This surface can either be described using a finite element model, or using a spring-mass system. The behaviors of the two models are similar.

not only provides us with a detailed description of the object's shape, but also tells us the intensity (albedo) of each point on the surface (ignoring, for now, the variation of shading with object orientation).

The surface model which we use is a finite element model, i.e., a collection of 3-D nodal variables roughly corresponding to the set of 3-D position measurements. This model can be viewed as either a true surface model composed of polygonal facets or simply as a neighborhood graph defined over the nodal variables (Figure 7). In either case, we start with the 3-D position measurements and add or remove points to obtain a smooth and continuous surface. Each point has a list of neighbors, which can be chosen either by finding the closest neighbors or by using the original topological relationship between the pixels that generated these points.

Generating a complete mesh for the surface from a sparse and scattered collection of points is in general quite difficult. For example, we could use Sha'ashua's [1988] Structural

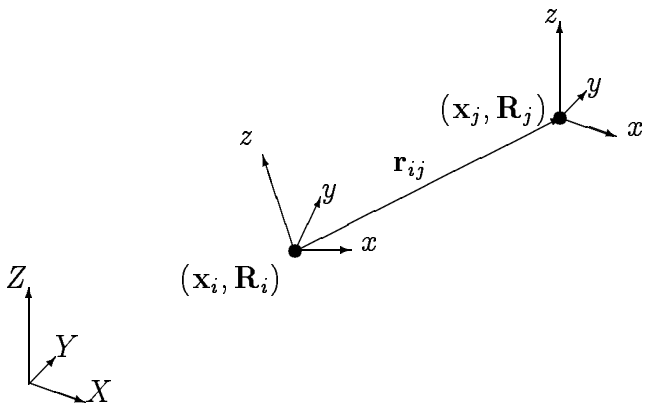

Figure 8: Oriented particle system with global and local coordinate frames.

Saliency theory, but this requires a dense (in this case 3-D) network of points, which would be computationally prohibitive. A simpler solution is to allow surface points to move into gaps in the surface. However, we have to be careful not to fill across true holes in the model, such as the handle in a cup (here, the bounding volume computed by [Szeliski, 1990] would be useful). Another possibility is to use the points on the surface of the bounding volume as candidates for mesh points.

To circumvent these difficulties, we have developed a new 3-D surface interpolation model based on interacting *oriented particles* [Szeliski and Tonnesen, 1991]. These particles, which represent local surface patches, have energy functions which favor the alignment of tangent planes of neighboring particles, thus endowing the surface with an elastic resistance to bending. The particles also have a preferred inter-particle spacing distance, which encourages a uniform sample density over the surface.

Each particle is represented by 6 state variables, 3 for position, and 3 for orientation (Figure 8). This is similar to the *Darboux frames* used by Sander and Zucker [1990], except that no local curvature information is kept. Within each particle's local coordinate frame, the energy function defining its interactions with other particles is

$$E_{ij} = (1 - \frac{r^2}{a^2}) \exp -\frac{1}{2}\left(\frac{r^2}{b^2} + \frac{z^2}{c^2}\right) \quad \text{where } r^2 = x^2 + y^2,$$

and $\mathbf{q}_{ij} = (x, y, z)$ is the local coordinate of particle j in particle i's coordinate frame,

$$\mathbf{q}_{ij} = \mathbf{R}_i^{-1} \wedge (\mathbf{p}_j - \mathbf{p}_i),$$

where $\mathbf{R}_i$ denotes the orientation of particle $\mathbf{p}_i$. In addition to the inter-particle smoothness forces, we use external forces to attract surface particles to the original sparse data [Szeliski, 1989].

Once a reasonably accurate surface model has been constructed, we can dispense with the optic flow computation altogether. As each new image arrives, it directly modifies the deformable surface model and its associated intensities by making small local changes which better register the model and the image. The data constraint energy between the surface model and the sparse data points is therefore replaced with a direct intensity matching energy

$$\mathcal{E}_{\mathrm{I}} = \frac{1}{2} \int \left[f(x(u,v), y(u,v)) - I(u,v) \right]^2 \left| \frac{\partial(x,y)}{\partial(u,v)} \right| du\, dv, \tag{18}$$

where $f(x, y)$ is the new image, $x(u, v)$ and $y(u, v)$ are the projected screen coordinates of the surface model, and $I(u, v)$ is its intensity.

6 Experimental results

We have performed a number of experiments with our shape from rotation algorithms on both live and off-line ("canned") image sequences. The experimental setup consists of a spring-wound microwave turntable with a position encoding grid taped to its side (Figure 1) and a stationary camera mounted on a tripod (General Imaging MOS-5300 Video Camera with a Fujinon 12.5-75mm TV zoom lens). A rough calibration of the intrinsic and extrinsic camera parameters can be obtained by locating the ellipse that defines the turntable top and measuring the camera to turntable distance. A more exact calibration can be obtained using multiple images of a calibration cube [Szeliski, 1990] (Figure 2a).

The live experiments involve building an octree bounding volume of the object, processing a 512×480 monochrome image every 3.4 seconds on a RISC-based workstation [Szeliski, 1990]. The algorithm is first adapted to the empty turntable while it is spinning, both to memorize the background, and to locate the position encoding ring. After the object is placed on the table, each new image is then thresholded and the turntable angle computed from the binary codes averaged over 32 columns (accurate to about $0.1°$). The bounding volume is then computed from the object silhouettes (Figures 2b–d).

For the off-line experiments, we first recorded onto videotape a number of image sequences of different objects spinning on the turntable (Figures 9–11a). We then digitized each sequence using the single-frame playback capabilities of our video recorder to obtain a high resolution image sequence of about 500 frames (about $0.72°$ rotation between frames). For the experiments presented in this paper, each image was subsampled from 512×480 to 256×240 with only every second frame being used. The resulting interframe rotation is about $1.44°$, with a maximum horizontal flow (on the turntable edge) of about 2.9 pixels.

These image sequences were input into our optic flow extraction algorithm, whose output was then backprojected into 3-D world coordinates. Figures 9, 10, and 11 show three of the image sequences we are using and the results of these initial depth extraction stages. The first image (a) in each figure shows the first frame of the input intensity image sequence. The second image (b) shows an intensity-coded depth map extracted from the first pair of images, where each local flow estimate has been converted to a screen-based depth value z (depth values with high uncertainty are not shown). The third image (c) shows the inverse variance (certainty) at each pixel. This certainty is much higher in textured areas and near strong intensity gradients. After eliminating the estimates whose variance is too large, we project the depth estimates into 3-dimensional position estimates. These are shown in the fourth part (d) of each figure, using a top view of the object to better see its structure (the wireframe cube and axes are for reference only). Both the circular structure of the turntable edge, and the rectangular structure of the tea box (Figure 9) and

the domino cube (Figure 11) are roughly recovered. The structure of the dodecahedron (Figure 10) is more difficult to see from the top view.

The next step in the shape from rotation algorithm consists of merging neighboring 3-D points acquired from different viewpoints. Figures 12, 13, and 14 show the results of this merging step, operating incrementally on the complete 250 image sequences. We present this data as isolated points shown in 4 different projections: top, front, side, and oblique. Unfortunately, it is somewhat difficult to gauge the true shape of the object using these flat two-dimensional projections. In our own experiments, we can rotate the object interactively to get a good sense of the depth and relationship of the points (kinetic depth effect). We also use multiple colors to display points from different iterations (when examining the merging step).

From these figures, we can see that the overall shape of the objects is recovered well, although the exact surface data is not very smooth. Adding a small amount of image-plane smoothing should help to reduce this effect [Matthies *et al.*, 1989]. Of course, once a complete surface model is fit to this sparse data, the resulting solution will also be smooth. Figures 13b–d show that in some cases, shadows will be incorporated into the object model (under many imaging and lighting geometries, the shadows form non-rigid structures, and are therefore discarded by the temporal integration stage). To remove these shadow points, we could either cut off the bottom of the model, or use a more sophisticated color-based image preprocessing stage. More detailed examination of the data reveals that even after integration over many frames, the depth estimates near horizontal edges are still poor. This suggests a bias in our flow estimator, which could be reduced either by using more temporal averaging (antialiasing), using using spatio-temporal filters [Fleet and Jepson, 1989], or using variable-sized windows [Okutomi and Kanade, 1990].

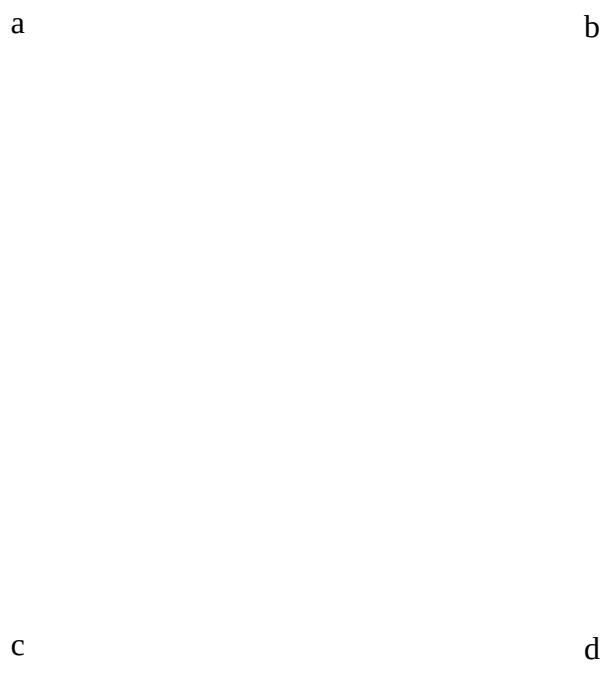

a b

c d

Figure 9: Flow computed from `assam` image series

(a) first image in sequence (b) depth map from flow (darker is nearer) (c) certainty in depth estimates σ_z^{-2} (darker is higher certainty) (d) top view of 3-D point cloud

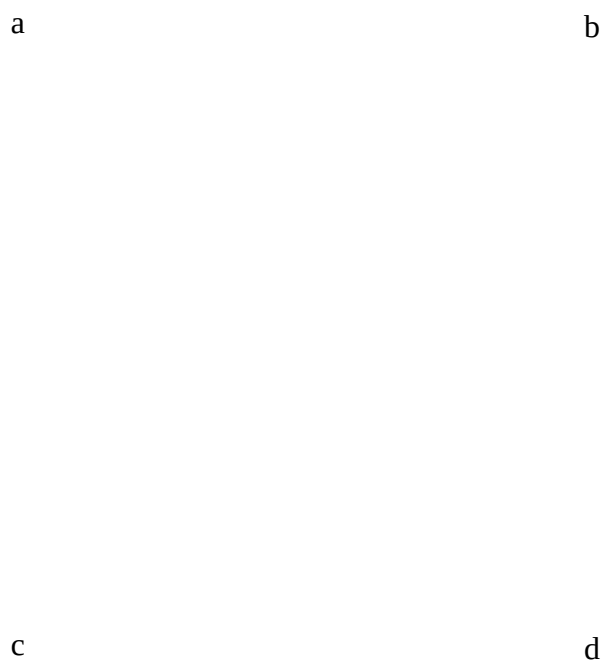

Figure 10: Flow computed from `dodecahedron` image series
(a) first image in sequence (b) depth map from flow (darker is nearer) (c) certainty in depth estimates σ_z^{-2} (darker is higher certainty) (d) top view of 3-D point cloud

a

c d

Figure 11: Flow computed from `domino` image series
(a) first image in sequence (b) depth map from flow (darker is nearer) (c) certainty in depth estimates σ_z^{-2} (darker is higher certainty) (d) top view of 3-D point cloud

a b c d

Figure 12: Final merged data from `assam` image series: (a) top view (b) oblique view (c) front view (d) side view

a b c d

Figure 13: Final merged data from `dodecahedron` image series: (a) top view (b) oblique view (c) front view (d) side view

a b c d

Figure 14: Final merged data from `domino` image series: (a) top view (b) oblique view (c) front view (d) side view

7 Discussion

The techniques we have described in this paper perform a shape construction task similar to that usually associated with active range sensors [Agin and Binford, 1976; Woodham, 1981; Besl and Jain, 1985]. An example of such a sensor, which can be used in short-distance indoor environments, is structured light, where an encoded light pattern falling on the object is used to give direct (and usually sparse) measurements of depth [Agin and Binford, 1976; Vuylsteke and Oosterlinck, 1990]. Compared to active range sensors, our approach requires a far less structured environment, since no special lighting sources are required, and the calibration of the system is simple and fairly automatic. Our technique also has the potential for better accuracy since our measurements are dense (at least in textured areas), and because we see more views of the object. On the other hand, our flow-based approach will fail in areas where the surface has a uniform albedo. An experimental comparison of these two techniques should be performed to better quantify these effects. Combining structured light with the shape-from-rotation paradigm should result in an algorithm that works under a wider variety of conditions, but at the expense of increased hardware complexity.

An alternative to the approach presented in this paper is to use the silhouette of the object in each frame to construct a bounding volume for the object [Szeliski, 1990]. This bounding volume can provide a non-linear (inequality) constraint on the position of surface points. Tracking the silhouettes through three or more images can also be used to estimate the location and curvature of points on the limb of the object [Giblin and Weiss, 1987; Vaillant, 1990; Cipolla and Blake, 1990]. Combining silhouette-based and flow-based approaches should yield an algorithm that works for a much wider variety of object shapes and textures.

Our shape from rotation algorithm would be even more useful if we could change the position of the camera and/or the object. The former case is easier to handle: we simply re-calibrate the system, and continue processing with the new camera parameters. The change

in object orientation caused by repositioning it on the turntable is also simple to handle if the new object pose is known. Determining this new pose from the surface data itself is more difficult. A three-dimensional generalization of an existing sparse range matching algorithm [Szeliski, 1988] should help us here.

Additional visual cues for reconstructing the object's shape should be added to our algorithm to make it more generally applicable and more robust. Shape from shading [Horn and Brooks, 1989] is a particularly interesting cue, since it provides information that is usually complementary to optic flow (it works best in uniform albedo areas). Specularities [Klinker *et al.*, 1988], which create difficulties for the current algorithm, would also be a powerful cue for shape computation [Healey and Binford, 1987]. To determine the lighting characteristics of our environment, we could use a reflective sphere or cube placed on the turntable during our calibration phase. While shape from shading and shape from specularities could be applied to a single image at a time, they may prove to be even more powerful when applied to a dynamic sequence.

The algorithm described in this paper builds a detailed locally parameterized surface model of the object. The next step in processing would be to build a higher-level description of the object, either for more efficient CAD/graphics manipulation, or for object recognition. An example of such a model would be a superquadrics parts model, which could be fitted directly to our sparse collection of 3-D points [Pentland, 1986]. However, if the part model does not fit the data well, we may wish to use something in between a finite element deformable model and a globally parameterized model, for example, a *deformable superquadric* [Terzopoulos and Metaxas, 1990]. This kind of model could also "snap" into a variety of preferred shapes such as cylinders or boxes [Terzopoulos and Metaxas, 1990].

8 Conclusions

Shape from rotation is a practical approach to building 3-D models from a sequence of images. The goal of this work is to produce a locally accurate model of shape and intensity of an unknown object, which could later be used to build a high-level parts description. As such, this technique should be useful in a variety of robotics and CAD tasks, as well as providing a novel source of objects for computer animation systems.

The design of our algorithm is motivated both by the increasing availability of massively parallel architectures for computer vision tasks, and the recent success of incremental algorithms in building high-quality depth maps from motion sequences. This work can be viewed as an extension of this recent work in $2\,{}^1\!/_2$-D incremental depth estimation to full 3-D shape reconstruction.

The design of a complete shape from rotation system requires the solution of a number of fundamental computer vision problems. These include flow estimation, uncertainty modeling, incremental estimation, 3-D surface representation and reconstruction, deformable (energy-based) models, and massively parallel algorithms. We have implemented and tested the main stages of processing (flow constraints, flow estimation, backprojection into 3-D, and 3-D point merging), but much interesting work remains to be done (surface reconstruction and refinement, evaluation, and enhancements). We expect that shape from rotation will prove to be an interesting and challenging problem to solve, as well as a good framework for studying various important computer vision techniques.

References

[Adelson and Bergen, 1985] E. H. Adelson and J. R. Bergen. Spatiotemporal energy models for the perception of motion. *Journal of the Optical Society of America*, A 2(2):284–299, February 1985.

[Agin and Binford, 1976] G. J. Agin and T. O. Binford. Computer description of curved objects. *IEEE Transactions on Computers*, C-25(4):439–449, April 1976.

[Anandan, 1989] P. Anandan. A computational framework and an algorithm for the measurement of visual motion. *International Journal of Computer Vision*, 2(3):283–310, January 1989.

[Anandan and Weiss, 1985] P. Anandan and R. Weiss. Introducing a smoothness constraint in a matching approach for the computation of displacement fields. In *Image Understanding Workshop*, pages 186–196, Science Applications International Corporation, Miami Beach, Florida, December 1985.

[Baker and Bolles, 1989] H. H. Baker and R. C. Bolles. Generalizing epipolar-plane image analysis on the spatiotemporal surface. *International Journal of Computer Vision*, 3(1):33–49, 1989.

[Besl and Jain, 1985] P. J. Besl and R. C.. Jain. Three-dimensional object recognition. *Computing Surveys*, 17(1):75–145, March 1985.

[Bolles *et al.*, 1987] R. C. Bolles, H. H. Baker, and D. H. Marimont. Epipolar-plane image analysis: an approach to determining structure from motion. *International Journal of Computer Vision*, 1:7–55, 1987.

[Broida and Chellappa, 1986] T. J. Broida and R. Chellappa. Kinematics of a rigid object from a sequence of noisy images: a batch approach. In *IEEE Computer Society Conference on Computer Vision and Pattern Recognition (CVPR'86)*, pages 176–182, IEEE Computer Society Press, Miami Beach, Florida, June 1986.

[Brooks *et al.*, 1979] R. A. Brooks, R. Greiner, and T. O. Binford. The ACRONYM model-based vision system. In *Sixth International Joint Conference on Artificial Intelligence (IJCAI-79)*, pages 105–113, Tokyo, Japan, August 1979.

[Burt, 1981] P. J. Burt. Fast filter transforms for image processing. *Computer Graphics and Image Processing*, 16:120–51, 1981.

[Chen and Huang, 1988] H. H. Chen and T. S. Huang. A survey of construction and manipulation of octrees. *Computer Vision, Graphics, and Image Processing*, 43:409–431, 1988.

[Cipolla and Blake, 1990] R. Cipolla and A. Blake. The dynamic analysis of apparent contours. In *Third International Conference on Computer Vision (ICCV'90)*, pages 616–623, IEEE Computer Society Press, Osaka, Japan, December 1990.

[Faugeras *et al.*, 1986] O. D. Faugeras, N. Ayache, and B. Faverjon. Building visual maps by combining noisy stereo measurements. In *IEEE International Conference on Robotics and Automation*, pages 1433–1438, IEEE Computer Society Press, San Francisco, California, April 1986.

[Fleet and Jepson, 1989] D. Fleet and A. Jepson. Computation of normal velocity from local phase information. In *IEEE Computer Society Conference on Computer Vision and Pattern Recognition (CVPR'89)*, pages 379–386, IEEE Computer Society Press, San Diego, California, June 1989.

[Giblin and Weiss, 1987] P. Giblin and R. Weiss. Reconstruction of surfaces from profiles. In *First International Conference on Computer Vision (ICCV'87)*, pages 136–144, IEEE Computer Society Press, London, England, June 1987.

[Hallam, 1983] J. Hallam. Resolving observer motion by object tracking. In *International Joint Conference on Artificial Intelligence*, 1983.

[Healey and Binford, 1987] G. Healey and T. O. Binford. Local shape from specularity. In *First International Conference on Computer Vision (ICCV'87)*, pages 151–160, IEEE Computer Society Press, London, England, June 1987.

[Heeger, 1987] D. J. Heeger. Optical flow from spatiotemporal filters. In *First International Conference on Computer Vision (ICCV'87)*, pages 181–190, IEEE Computer Society Press, London, England, June 1987.

[Heel, 1990] J. Heel. *Direct Estimation of Structure and Motion from Multiple Frames*. A.

I. Memo 1190, Artificial Intelligence Laboratory, Massachusetts Institute of Technology, March 1990.

[Hennessy and Patterson, 1990] J. L. Hennessy and D. A. Patterson. *Computer Architecture: A Quantitative Approach*. Morgan Kaufmann Publishers, Los Altos, California, 1990.

[Hillis, 1985] W. D. Hillis. *The Connection Machine*. MIT Press, Cambridge, Massachusetts, 1985.

[Horn, 1990] B. K. P. Horn. Relative orientation. *International Journal of Computer Vision*, 4(1):59–78, January 1990.

[Horn and Brooks, 1989] B. K. P. Horn and M. J. Brooks. *Shape from Shading*. MIT Press, Cambridge, Massachusetts, 1989.

[Horn and Schunck, 1981] B. K. P. Horn and B. G. Schunck. Determining optical flow. *Artificial Intelligence*, 17:185–203, 1981.

[Hutchinson *et al.*, 1988] J. Hutchinson, C. Koch, J. Luo, and C. Mead. Computing motion using analog and binary resistive networks. *Computer*, 21(3):52–63, March 1988.

[Jackins and Tanimoto, 1980] C. L. Jackins and S. L. Tanimoto. Oct-trees and their use in representing three-dimensional objects. *Computer Graphics, and Image Processing*, 14:249–270, 1980.

[Klinker *et al.*, 1988] G. J. Klinker, S. A. Shafer, and T. Kanade. The measurement of highlights in color images. *International Journal of Computer Vision*, 2(1):7–32, June 1988.

[Koch *et al.*, 1986] C. Koch, J. Marroquin, and A. Yuille. Analog "neuronal" networks in early vision. *Proceedings of the National Academy of Sciences U.S.A.*, 83:4263–4267, June 1986.

[Little *et al.*, 1989] J. Little, G. E. Blelloch, and T. A. Cass. Algorithmic techniques for

computer vision on a fine-grained parallel machine. *IEEE Transactions on Pattern Analysis and Machine Intelligence*, PAMI-11(3):244–257, March 1989.

[Lucas, 1984] B. D. Lucas. *Generalized Image Matching by the Method of Differences*. PhD thesis, Carnegie Mellon University, July 1984.

[Matthies and Shafer, 1987] L. Matthies and S. A. Shafer. Error modeling in stereo navigation. *IEEE Journal of Robotics and Automation*, RA-3(3):239–248, June 1987.

[Matthies and Kanade, 1987] L. H. Matthies and T. Kanade. The cycle of uncertainty and constraint in robot perception. In *International Symposium on Robotics Research*, MIT Press, August 1987.

[Matthies *et al.*, 1989] L. H. Matthies, T. Kanade, and R. Szeliski. Kalman filter-based algorithms for estimating depth from image sequences. *International Journal of Computer Vision*, 3:209–236, 1989.

[Meagher, 1982] D. Meagher. Geometric modeling using octree encoding. *Computer Graphics, and Image Processing*, 19:129–147, 1982.

[Nagel, 1987] H.-H. Nagel. On the estimation of optical flow: relations between different approaches and some new results. *Artificial Intelligence*, 33:299–324, 1987.

[Newman and Sproull, 1979] W. M. Newman and R. F. Sproull. *Principles of Interactive Computer Graphics*. McGraw Hill, New York, New York, 2 edition, 1979.

[Okutomi and Kanade, 1990] M. Okutomi and T. Kanade. A signal matching algorithm: an adaptive window based on a brownian motion model. In *Third International Conference on Computer Vision (ICCV'90)*, pages 190–199, IEEE Computer Society Press, Osaka, Japan, December 1990.

[Pentland, 1986] A. P. Pentland. Perceptual organization and the representation of natural form. *Artificial Intelligence*, 28(3):293–331, May 1986.

[Poggio *et al.*, 1985] T. Poggio, V. Torre, and C. Koch. Computational vision and regular-

ization theory. *Nature*, 317(6035):314–319, 26 September 1985.

[Rives *et al.*, 1986] P. Rives, E. Breuil, and B. Espiau. Recursive estimation of 3D features using optical flow and camera motion. In *Conference on Intelligent Autonomous Systems*, pages 522–532, Elsevier Science Publishers, December 1986. Also appeared in 1987 IEEE International Conference on Robotics and Automation.

[Sander and Zucker, 1990] P. T. Sander and S. W. Zucker. Inferring surface trace and differential structure from 3-D images. *IEEE Transactions on Pattern Analysis and Machine Intelligence*, 12(9):833–854, September 1990.

[Sha'ashua and Ullman, 1988] A. Sha'ashua and S. Ullman. Structural saliency: the detection of globally salient structures using a locally connected network. In *Second International Conference on Computer Vision (ICCV'88)*, pages 321–327, IEEE Computer Society Press, Tampa, Florida, December 1988.

[Szeliski, 1988] R. Szeliski. Estimating motion from sparse range data without correspondence. In *Second International Conference on Computer Vision (ICCV'88)*, pages 207–216, IEEE Computer Society Press, Tampa, Florida, December 1988.

[Szeliski, 1989] R. Szeliski. *Bayesian Modeling of Uncertainty in Low-Level Vision*. Kluwer Academic Publishers, Boston, Massachusetts, 1989.

[Szeliski, 1990] R. Szeliski. *Real-Time Octree Generation from Rotating Objects*. Technical Report 90/12, Digital Equipment Corporation, Cambridge Research Lab, December 1990. For ordering information, please send a message to techreports@crl.dec.com with the word `help` in the Subject line.

[Szeliski and Ito, 1986] R. Szeliski and M. R. Ito. New Hermite cubic interpolator for two-dimensional curve generation. *IEE Proceedings E*, 133(6):341–347, November 1986.

[Szeliski and Tonnesen, 1991] R. Szeliski and D. Tonnesen. Particle systems for surface interpolation. *Computer Graphics (SIGGRAPH'91)*, (in preparation) 1991.

[Terzopoulos and Metaxas, 1990] D. Terzopoulos and D. Metaxas. Dynamic 3D models with local and global deformations: deformable superquadrics. In *Third International Conference on Computer Vision (ICCV'90)*, pages 606–615, Osaka, Japan, December 1990.

[Terzopoulos *et al.*, 1987] D. Terzopoulos, A. Witkin, and M. Kass. Symmetry-seeking models and 3D object reconstruction. *International Journal of Computer Vision*, 1(3):211–221, October 1987.

[Tomasi and Kanade, 1990] C. Tomasi and T. Kanade. Shape and motion without depth. In *Third International Conference on Computer Vision (ICCV'90)*, pages 91–95, IEEE Computer Society Press, Osaka, Japan, December 1990.

[Ullman, 1984] S. Ullman. Maximizing rigidity: the incremental recovery of 3-D structure from rigid and nonrigid motion. *Perception*, 13:255–274, 1984.

[Vaillant, 1990] R. Vaillant. Using occluding contours for 3D object modeling. In *First European Conference on Computer Vision (ECCV'90)*, pages 454–464, Springer-Verlag, Antibes, France, April 23–27 1990.

[Vuylsteke and Oosterlinck, 1990] P. Vuylsteke and A. Oosterlinck. Range image acquisition with a single binary-encoded light pattern. *IEEE Transactions on Pattern Analysis and Machine Intelligence*, PAMI-12(2):148–164, February 1990.

[Woodham, 1981] R. J. Woodham. Analysing images of curved surfaces. *Artificial Intelligence*, 17:117–140, 1981.

A Inverse perspective projection with homogeneous coordinates

To compute the world (object) coordinates of a point $\mathbf{p}$ given its screen coordinates $\mathbf{q}$, we can use the projection operator $\mathcal{P}$ *after* the inverse matrix transformation $\mathbf{M}^{-1}$. To see that this is the case, we note from (4) that

$$\mathbf{p}' = W'\mathbf{q}$$

where the value of W' is unknown. From (3) we have

$$\mathbf{p} = \mathbf{M}^{-1}\mathbf{p}' = W'\mathbf{M}^{-1}\mathbf{q}.$$

But since we know that the fourth element of $\mathbf{p} = (X, Y, Z, 1)$ was originally 1, we can simply normalize $\mathbf{M}^{-1}\mathbf{q}$ to obtain the formula in (5)

$$\mathbf{p} = \mathcal{P}\left(\mathbf{M}^{-1}\mathbf{q}\right).$$

Similarly, if we wish to determine where the pixel at time t denoted by screen coordinates $\mathbf{q}_t$ was at time $t-1$ (denoted by $\mathbf{q}_{t-1}$), we have

$$\mathbf{p} = W'_t\mathbf{M}_t^{-1}\mathbf{q}_t$$

and

$$\mathbf{q}_{t-1} = \mathcal{P}\left(\mathbf{M}_{t-1}\mathbf{p}\right) = \mathcal{P}\left(\mathbf{M}_{t-1}\mathbf{M}_t^{-1}\mathbf{q}_t\right)$$

(since the projection operator is invariant to a uniform scaling of its input). Thus, even for composite transformations of coordinates, we only have to perform one projection operation at the end of the transformation, even if multiple perspective or inverse perspective transformations have occured.

Acknowledgements

I would like to thank Gudrun Klinker for her careful reading of this manuscript and many helpful suggestions, and an anonymous CVPR’91 reviewer for his detailed comments and insightful observations.